



High End Corrosion and Wear Behavior of HA-CNT Coatings on Biomaterials

¹Mahesh M Sonekar & ²Walmik S Rathod

¹PhD Scholar & ²Associate Professor, Department of Mechanical Engineering, Veermata Jijabai Technological Institute, Mumbai, INDIA-400 019

ABSTRACT:

The present study deals with the critically evaluation of the corrosion and wear behavior of bare and as sprayed reinforced HA-CNT coatings on SS-316L, CoCrMo and Ti6Al4V alloy substrates. Corrosion behavior of all coatings was evaluated by electrochemical polarization test in simulated body fluid as proposed by Kokubo and Takadama. To evaluate wear behavior of all the sprayed pure and reinforced HA-CNT coatings, a wear tester was fabricated as proposed by Morks et al. In case of bare and coated substrates the results of Tafel polarization test have shown that Ti6Al4V alloy has superior corrosion resistance in simulated body fluid solution as compared to SS-316L and CoCrMo alloy. Potentiodynamic curves show that all the alloys show passive behavior but Ti6Al4V has more passive region. The present study also looks at dry and wet unidirectional sliding wear behaviors, as well as the influence of incorporating carbon nanotubes (CNTs) in different weight percent to hydroxyapatite (HA) by plasma spraying on its tribological properties. Crystallinity and volume percent with open porosity were substantially higher in the APS-CNT imposed HA coating than in the control. When compared to pure HA coating, the enhanced hardness ranged from 2.4 to 5.6 GPa, the modulus of elasticity ranged from 105 to 172 GPa, and the fracture toughness from 0.6 to 2.4 MPa.m^{1/2}, with a reduced wear rate of 50.2x10⁻⁵ mm³ to 4.2x10⁻⁵ mm³ N⁻¹ m⁻¹ because of the release of graphene layer from CNT surface, which acts as a lubricant. The outcomes showed that adding carbon nanotubes (CNTs) to the coating enhanced tribological behaviour as well as corrosion resistance. These advancements have been credited to nanotubes' exceptional mechanical capabilities, distinctive topological structure, and high degree of chemical stability.

Keywords: Biomaterial, Characterization, Coating, Corrosion, Air Plasma Spray, Wear, Tribology, Polarization.

DOI Number: 10.14704/nq.2022.20.8.NQ44864

NeuroQuantology 2022; 20(8): 8407-8423

1. INTRODUCTION

The degradation of a metal by corrosion processes that happen either directly or indirectly as a result of the activity of living organisms is known as biological corrosion. These organisms come in both micro and macro varieties, such as bacteria, algae, and barnacles. Chemical reactions keep living things alive. In other words, organisms consume a reactant or food and excrete waste. According to [1], these

processes can influence corrosion behaviour in the following ways:

1. By having a direct impact on cathodic and anodic reactions.
2. By directly affecting surface-protective coatings
3. By producing toxic circumstances
4. By creating a deposit.

The human body depends on a large number of chemical reactions occurring continuously to sustain

8407



it viability. These chemical reactions produce an abundance of oxidizing agents, which creates an unfriendly environment for metals and alloys. Even immune to the forces of nature and undergo some of the most corrosion-resistant materials are not degree of corrosion [2]. All metals used for human implantation initially corrode and form a thin barrier film. The barrier film formed on the surface of the newly implanted metal offers a chemical barrier to corrosion and prevents the degradation of deeper metal atoms. Without this barrier, the metals would react violently with the surrounding chemical environment and eventually dissolve. Mechanical forces can disrupt this layer which then leaves reactive metal atoms susceptible to corrosion. Corrosion is one of the major cause problems when metals and alloys are used as implants in the body [3]. Corrosion of implants in the aqueous medium of body fluids takes place via electrochemical reactions and it is necessary to appreciate and understand the electrochemical principles that are most relevant to the corrosion processes. The electrochemical processes that take place on the alloy's surface after surgery are the same as those that are seen when it is exposed to seawater (namely, aerated sodium chloride). The dissolved oxygen is reduced to hydroxyl ions and the metallic alloy's constituent parts are oxidized to take on their ionic forms. The total rates of oxidation and reduction reactions, which are known as electron generation and electron consumption, must be equal during the corrosion process. The slower of these two processes governs the overall reaction rate. Pitting, crevice, galvanic, intergranular, corrosion fatigue, and fretting corrosion are the types of corrosion that are relevant to the currently utilized alloys [4].

The primary criteria for a bioimplant should be its biocompatibility with the biological system, strong mechanical capabilities to bear varied loads caused, and exceptional corrosion resistance in the bodily fluid [5]. Metals and alloys, polymers, ceramics, and reinforced composites are the many types of materials used in bio-implants. The most often utilized implant materials are cutting-edge materials with good biomechanical qualities, such as surgical

stainless steel, CoCrMo alloys, and various Titanium grades. However, their principal drawback is that they could not always be biocompatible with bodily fluids, and tissues might not develop on them once they are implanted in the body [6]. Traditional orthopedic implant production materials frequently failed due to a lack of or insufficient integration of implant materials to the adjacent bone and stress-strain imbalance at the tissue-implant material interface [7]. Despite the various benefits of hydroxyapatite coating on metallic substrates, clinical trials are delayed under different loading circumstances due to the brittleness and low strength of hydroxyapatite [8]. Since HA is fragile, secondary reinforcing elements such Zirconia, Ni3Al, Alumina (Al_2O_3), carbon nanotubes (CNTs), boron nitride nanotubes (BNNTs), Silica, and Ti-grade alloys are frequently utilized to enhance mechanical qualities like fracture toughness and Young's modulus [9]. In terms of biological and tribo mechanical properties, CNT reinforced composites fared better than other composites. The biological properties, crystallinity, and form of HAP are improved by the inclusion of CNTs [10]. A composite's COF can be decreased by altering the rate of CNT. CNTs are added, which promotes cell attachment and proliferation. There are reductions in wear-related mass loss of 13.33, 66.67, and 83.33 percent [11]. The inherent nature of CNTs, including their physical and chemical properties, is explained in order to comprehend the functionalization of CNTs to improve their hydrophobic properties. To boost dispersity in aqueous environments and reduce toxicity, CNTs are frequently functionalized with various functional groups (such as -OH and -COOH) utilising covalent and non-covalent techniques [12]. The biocompatibility of Ti-Co-Cr is more distinctive due to the presence of titanium metal, as shown by the specimens' resistance to corrosion [13]. Plasma sprayed Al_2O_3 - TiO_2 ceramics have numerous uses in the aerospace, textile, and automotive industries for corrosion, wear, and abrasion resistance [14]. Gell et al. [15] researched plasma-sprayed 13 weight percent Al_2O_3 - TiO_2 coatings with nanostructures, and they found that



the US Navy had given the coatings the go-ahead for use on submarines and shipboards.

It is generally known that HA coating wear can lead to the degeneration or failure of orthopedic implants. The key factor affecting the longevity of total joint replacements, according to prior studies, is "worn particle-induced osteolysis, particularly near to acetabular components" [16]. The articulating surface generates wear particles that travel along the implant interface and lead to osteolysis, implant loosening, and ultimately implant failure. On the mechanism of micro-structural breakdown, there was, however, no comprehensive information. It takes a lot of work to investigate the microstructure level tribological behaviour of HA-CNT coated specimens. Due to inconsistent results from toxicological experiments due to a lack of standardization, the impact of CNTs on the human body and the environment is not well documented [17]. The current project will look at the micro structural characteristics of applied coatings and the possibility of plasma-sprayed HA-CNT coating for bioimplant applications. In order to determine their potential for in vivo applications, an attempt was made in this work to deposit HA with 10% and 5% CNT on surgical grade SS 316L, CoCrMo, and Ti6Al4V substrates.

The corrosion and wear properties of bio-inert metallic materials have previously been studied, including Ti-based alloys [18, 19] Co-based alloys [20], stainless steel [21], and Ti-Ni shape memory alloys [22]. There hasn't been much research on the corrosion and wear properties of HA-CNT coated with various weight percent degradable alloys; instead, the majority of studies have focused on

their general mechanical properties and corrosion properties. It is crucial to investigate the wear and corrosion properties of HA-CNT coated alloy. The goal of the current study is to analyze the corrosion and wear behaviour of biomaterials with HA-CNT coatings. Additionally, comparisons are made between the wear resistance and corrosion and tribocorrosion behaviors of several metallic-based alloys.

2. EXPERIMENTAL PROCEDURE

2.1 Powder coating methods for substrate and feedstock preparation: The alloy samples of SS 316L, CoCrMo, and Ti6Al4V were cut into a disc-like shape with a 40x5 mm estimated diameter. For improved adhesion of coating powders, the surface of coated samples is prepared using alumina (Al₂O₃) of size 65-90 m in a grit blaster within a blasting pressure range of 0.50 MPa. Before applying the final coating, the samples were air-blasted after grit blasting to remove any alumina contamination. The chemical make-up of HA-CNT powder for coating substrate materials is shown in Table 1. Commercially accessible HA powder from the Chinese company Xi'an Prius Biological Engineering Co., Ltd. was utilized for coating deposition, and MWCNT from the Indian company Adnano Technologies Pvt Ltd., Karnataka, was employed as reinforcing material. At Plasma Spray Coats, Bangalore, India, the reinforcing material was uniformly mixed with pure hydroxyapatite powder in proportions of 10% and 5% by weight using a laboratory ball mill for up to ten hours. Table 1 displays the particle size, content (in weight percent), and powder identification.

8409

Table 1. Chemical composition and other details of HA-CNT coating powder.

Coating Powder	Composition (Wt. %)	Particle size	Designation
Pure HA	Ca ₁₀ (PO ₄) ₆ OH ₂	100 – 180 μm	Pure HA
Reinforced HA	Ca ₁₀ (PO ₄) ₆ OH ₂ - MWCNT (10wt% & 5wt %) mixed in laboratory ball mill for 8 hrs.	Reinforcement 10 – 55 μm	Reinforced HA-C

When deciding on the criteria for various wt% of HA-CNT coating and tribological analysis, the wear circumstances of an orthopaedic implant inside the human body were taken into account. The hip joint

is one of the main load-bearing regions that encounters significant frictional forces when moving. HA is frequently applied to the stem and acetabular cup of the femoral component of the hip



joint. Compared to the femoral head's mating surface and the acetabular cup's interior, these areas are subject to significantly less friction. The wear parameters for this inquiry were selected based on the wear circumstances the femoral head encounters inside the acetabular cup. Hip joints are put to 0.85 to 2.57 MPa of pressure while walking. It is hoped that 38 HA coating will be able to withstand high frictional loads. Scanning electron micrographs have been used to study the morphology of hydroxyapatite powder that has carbon nanotube reinforcement on coated metal substrates. The Xta-LABmini™ Benchtop X-ray Diffraction/Crystallography system from Rigaku Americas Corporation was used to characterise these powders in the angle range of 20 to 90. The micrographs and EDX analysis of the (10wt percent and 5wt percent) reinforced HA-C coating are shown in Figure. 1(a & b) and Table. 2. The reinforced material has crushed angular and

spherical shapes, as shown on the SEM micrograph. The 10wt% coated sample has the greatest and most obvious wear debris, while the 5wt% coated sample has the least amount and shows delamination of wear debris. EDS examination can confirm a little amount of oxide and a small amount of wrecked debris. Figure 1(a&b) display the results of the EDS analysis of alloys with 10 weight percent and 5 weight percent HA-CNT coatings under dry and wet sliding conditions. The results of the EDS analysis reveal that the content of other elements (such as element O) besides Fe is higher in the wear debris than it is in the wear scar in the other samples that can produce wear debris. The O concentration in the 5 weight percent wear debris is lower than the wear scar, though. EDS examination revealed that the primary constituents in the corrosion products—Fe, O, P, W, and Ca—might be phosphates and hydroxide.

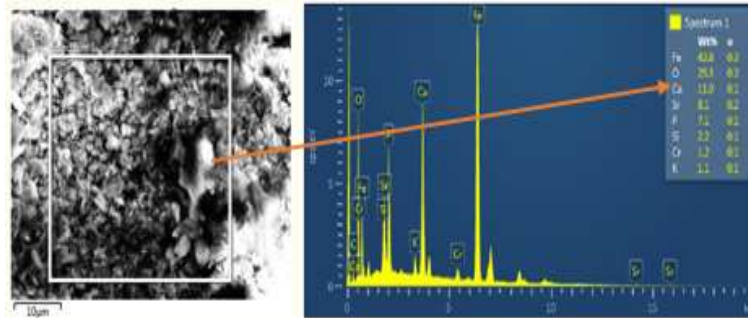


Figure. 1 (a) Scanning electron micrograph showing morphology of (10wt %) reinforced HA-CNT powder.

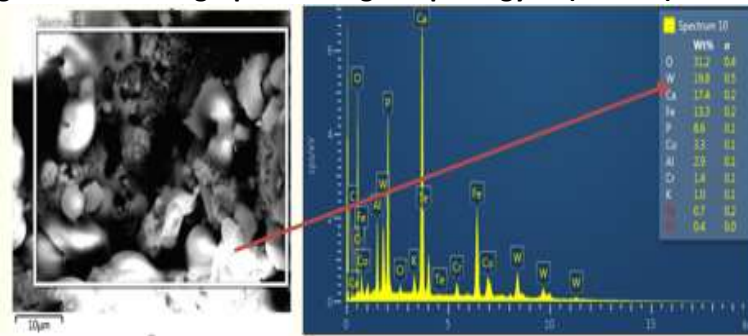


Figure.1 (b) Scanning electron micrograph showing morphology of (5wt %) reinforced HA-CNT Powder.

2.2 Wear Analysis: To examine abrasive wear, bare and HA-CNT coated samples were slide under dry and wet (SBF) conditions using a ball/pin on disc tribo tester (Ducom Instruments, model TR-20LE).

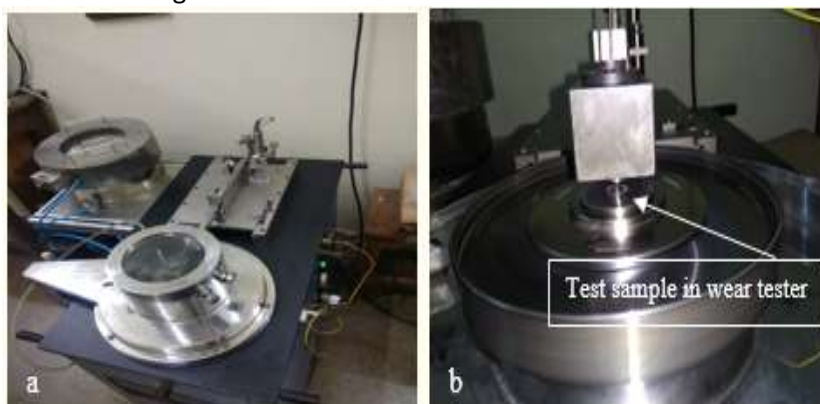
The samples were made in accordance with G95-99a. To examine the equivalent, the influence of the Alumina Ball's counter body was investigated. The testing samples' roughness (Ra) values were



made in the range of 0.8 m or less. The wear at a macro level was studied using a variable speed of 100 RPM with a 25 mm circular track radius and a total travelling distance of 90 - 200 m. The tribo probe's linear speed was predetermined to be 10 mm/s. An 8 mm diametric counter body (probe) was employed. An 8 mm diametric Alumina ball was utilized as the counter body (probe). The built-in LVDT sensor calculates the linear force between a coated surface and a steel probe that is positioned beneath a worn track to determine its depth. At a frequency level of 17 Hz, measurements on the coefficient of friction are collected. The wear track profiles on the tested samples were obtained using an Alicona 3D profilometer. Utilizing the wear track

depth profile, the value of wear volume is calculated.

The visual picture of a wear (tribological) research under physiological settings is shown in Figure 2. The tests were conducted using samples submerged in externally supplied simulated bodily fluid (SBF) under the same test circumstances and parameters as the dry wear test in the tribo tester [23], a substance having the same ion concentration of molecules as human blood, is used to make and sell the SBF at KET's Scientific Research Centre in Mumbai, India. These fluids are appropriate for evaluating the corrosion resistance since the chloride ions induces corrosion in biomaterials [24].



8411

Figure. 2 Experimental set-ups for tribological wear test (a) wear testing machine (b) wear test sample in physiological condition.

2.3 Coating Characterization: CoCrMo, Ti6Al4V, and SS 316L substrates coated with 10% and 5% CNT and worn-out surfaces have all been subjected to critical analysis. Under the ZEISS Gemini field emission scanning electron microscope (FE-SEM), which operates at 18 kV, the metallographic analysis of the coatings as they are sprayed on these substrates is investigated. Prior to SEM analysis, gold is used as the sputter coating material to enable high-resolution imaging. The optical micrograph in Figure 3 shows that the coating's top surface is devoid of cracks and macro-level porosity. The majority of the splats shows no signs of disintegration and is well-formed. In the majority of

the micrographs, some melted grains can also be seen on the surface of coatings. Furthermore, it is clear from the SEM/EDX study that Ca-rich HA particles are responsible for a whitish appearance in the coating that can be seen in SEM micrographs. Some streaks are found in reinforced HA coatings; EDX analysis of these streaks reveals that reinforcing content is present and spread throughout the matrix of the HA-C coatings [25, 26]. Calcium phosphate deposits had a Ca/p ratio of 1.62, which is comparable to the ratio of 1.64 in real bone, according to ED's spectroscopy [27, 28].



Element wt %	Composition (5 wt %)
W	30.6
O	.8
Ca	16.8
P	10.3
Cr	5.2
Co	4.4
K	2.6
Sr	1.7
Fe	0.9
Zn	0.8
Ni	0.7
Ti	0.3

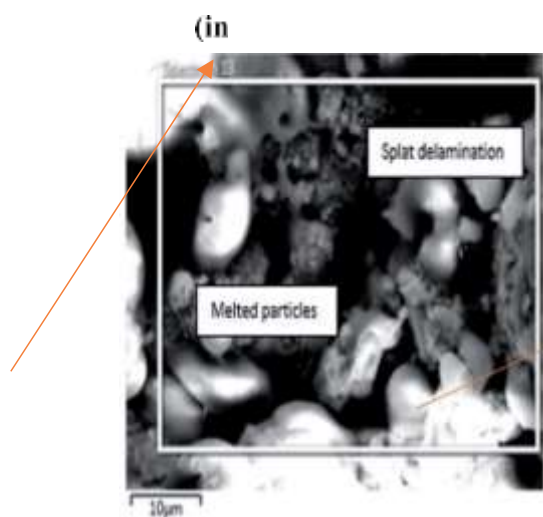
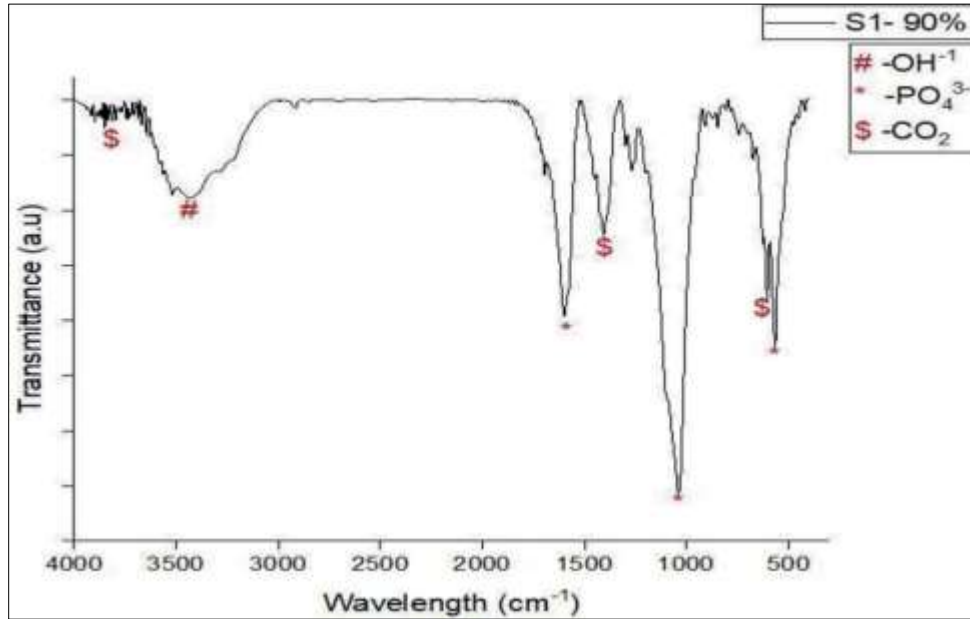


Figure. 3 Optical micrograph of reinforced HA-C coating on Ti6Al4V alloy

Figure 4 provides information on the FTIR examination of coated samples with HA-CNT reinforcement in the 4000 to 500 cm^{-1} range. When PO_4^{3-} group is present at 960 cm^{-1} , 1033 cm^{-1} , and 558 cm^{-1} , the OH- group at 3568 cm^{-1} and 652 cm^{-1}

can be seen. At 2360 cm^{-1} , CO_2 molecules that were not visible in the initial powder can now be seen. In the case of reinforced HA-C coatings on all alloy substrates, the intensity of the OH- group has diminished in comparison to before coating.

Figure. 4 FTIR spectroscopy for plasma sprayed reinforced HA-C coating powder (a) 10wt% CNT



8413

Micro hardness is the fundamental mechanical characteristic of HA-C coating, which may be crucial in the application of bio implants. The micro hardness of coatings on alloy substrates was assessed at the coating interface. The profiles for micro hardness with distance from the coating substrate interface are shown in Figure 5. The hardness of both (10wt percent & 5wt percent)

reinforced HA-C coating is lowest at the interface in case of all three alloy substrates (310 Hv, 340 Hv, and 402 Hv in case of uncoated SS 316l, CoCrMo, and Ti6Al4V, respectively; 322 Hv, 352 Hv, and 418 Hv in case With the reinforcing content, a little increase in hardness was seen. A 5 percent HAP/MWCNT coating had better hydrophobicity due to increased Vickers hardness [29].



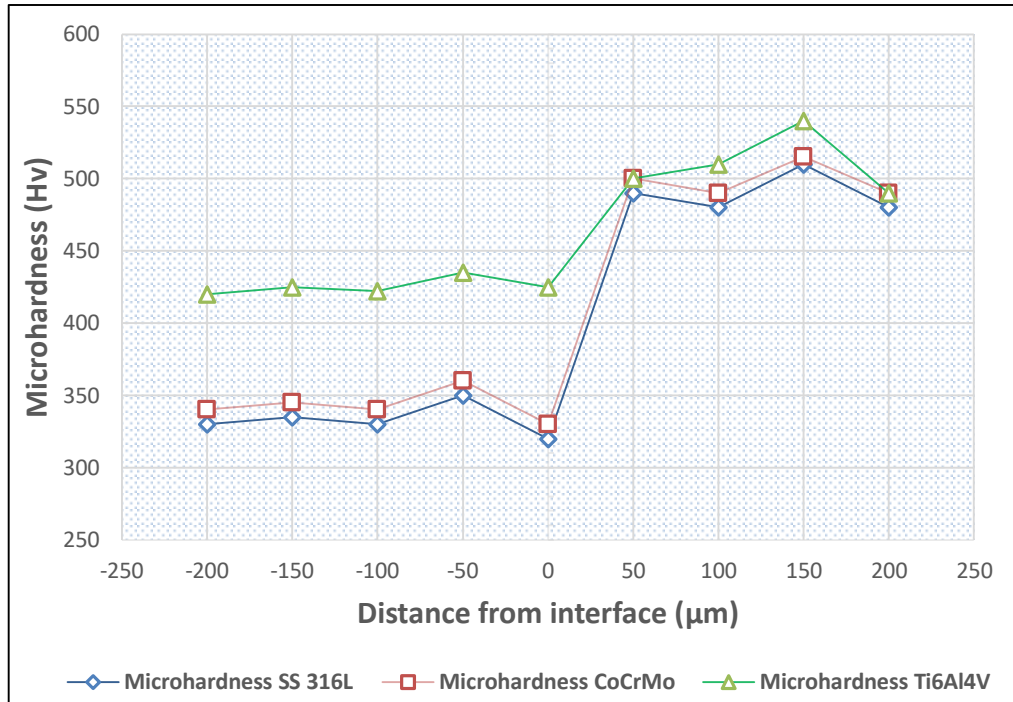


Figure. 5 Micro hardness profiles of reinforced HA-C coatings on SS 316L, CoCrMo, and Ti6Al4V alloy along the cross section

2.4 Corrosion (Electrochemical Polarization) Test:

In aqueous solutions, electrochemical mechanisms often dominate corrosion degradation. In order to comprehend the researched materials' corrosion behavior in simulated bodily fluids, the electrochemical reaction that was occurring on them was carefully observed. The electrochemical cell has three electrodes. The examined material served as the working electrode in the electrochemical cell, which also included a platinum wire serving as the counter electrode and an Ag/AgCl electrode serving as the reference electrode.

2.4.1 Cyclic polarization tests: The pace of electrochemical processes is frequently investigated using cyclic polarization tests over a range of potentials. Additionally, this method is frequently used to examine a passive material's susceptibility to localized corrosion start [30]. This research uses cyclic polarization tests to examine the corrosion and tribocorrosion behavior of bare and coated SS-316L, CoCrMo, and Ti6Al4V alloys. Figure 6 depicts the usual cyclic polarization curve of a passive metal. First, the examined material's potential is

elevated in the anodic direction. The working electrode transforms into a net anode for potential values higher than the corrosion potential (E_{corr}), allowing the investigation of the rate of charge transfer as a function of potential. As the potential is raised more, the material's passivity may be impaired. The current density abruptly increases due to the breakdown of the passive layer at the breakdown potential (E_b). The potential scan is reversed and the sample is polarized in the cathodic direction when current density reaches a predetermined level (or when the potential reaches a specific level without breakdown). The corrosion pits repassivation is determined by the repassivation potential (E_r).

2.4.2 Open circuit potential tests: Since the anodic reaction rate and the cathodic reaction rate are equal at the open circuit potential (OCP), there is no net current. OCP tests offer a qualitative assessment of a metal's condition (active or passive) in a specific setting. OCP can also be researched while materials are being mechanically loaded and worn out, as shown in Figure 7. Damage to the passive layer in the case of passive materials may

8414



reveal the underlying material and cause the OCP to decrease in value, moving toward higher active values. On the other hand, when mechanical damage stops, the passive layer repassivation, producing higher and more passive OCP values. To

examine the behavior of bare and coated substrates under tribocorrosion and fretting-corrosion conditions, open circuit potential tests have been carried out.

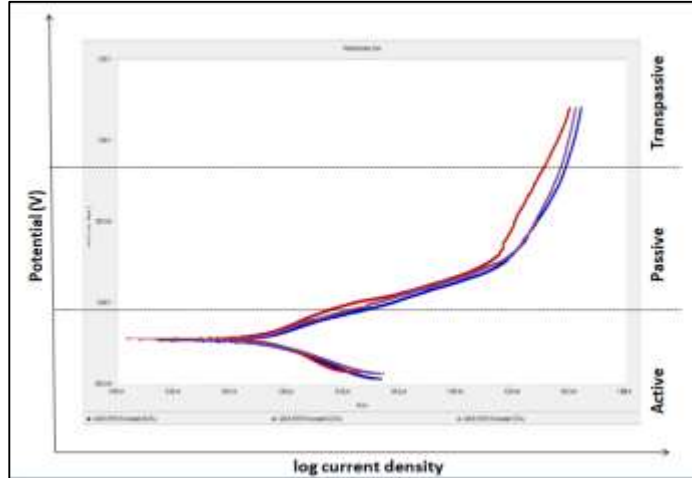


Figure 6 Typical cyclic polarization curves for passive corrosion behaviour

2.4.3 Potentiostatic tests: During potentiostatic studies, which apply a constant potential to the substance under investigation, the rate of charge transfer can be quantified. The mechanical and electrochemical repassivation of a passive metal under wear-corrosion circumstances can be studied by applying a voltage in the material's passive range. Another method of investigating the

repassivation process is to examine the recovery of the passive currents after the mechanical damage has ceased. Potentiostatic experiments have been used to examine the fretting corrosion performance of coated and uncoated samples as well as the effects of potential and solution chemistry on the tribocorrosion performance of materials.

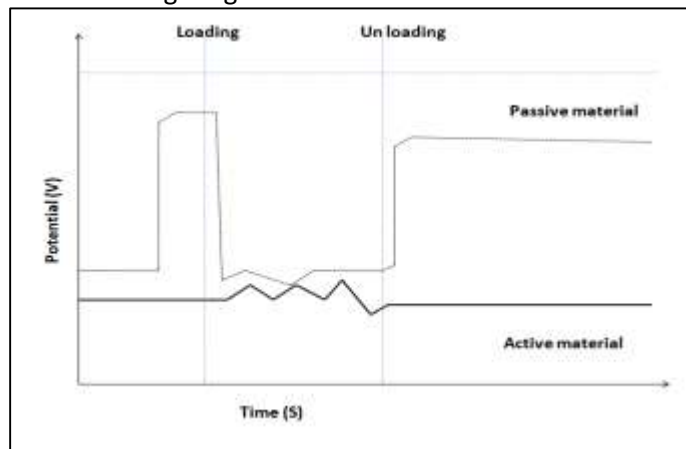


Figure 7 Schematic of behaviour of the open circuit potential of a material (solid line) and a passive material (dotted line) under tribocorrosion conditions.

3. RESULT AND DISCUSSION

3.1 Characterization of uncoated and plasma sprayed HA-C reinforced coating: Figure 8(a) showed that the surgical stainless steel SS-316L had

equiaxed austenite grains that were consistent with the steel's grade [31]. (ASTM Handbook 2001). The structure also includes annealing twins, demonstrating its similarity to the structure



described in the guidebook. Austenitic stainless steel with a 0.03 percent maximum carbon concentration is known as SS-316L. This steel develops a carbide-free austenitic and strain-free microstructure at annealing temperatures of 1010°C to 1065°C (1700 to 1850 °F), which retains in the soluble carbon due to quick quenching. CoCrMo alloy has a hexagonal close-packed, face-centered cubic crystalline structure, as shown in Figure 8(b). The face-centered cubic phase is often dominant at room temperature, resulting in the transition of fcc to hcp. The larger, hcp-structured Co dendrites that make up the micro structural grain are surrounded by smaller, M23C6-type carbides that are embedded in them. According to the analysis, there

is fine grain structure and homogeneous porosity. In fig. 8(c), the standard microstructures from the Metals Handbook (1975) and the ASM Handbook (1992, 2001). Equiaxed grains and intergranular structures make up the microstructure, which is consistent with the alloy's grade. The CA/P ratio, which is the ratio sought for long-term uses of the implant, is confirmed by EDAX analysis to be in the range of 1.67-2.4 [32]. Because SBF contains more calcium ions, has a larger negative charge, and has more accessible nucleation sites, CNT -HA composites can produce bone-like apatite on the surface of the sample

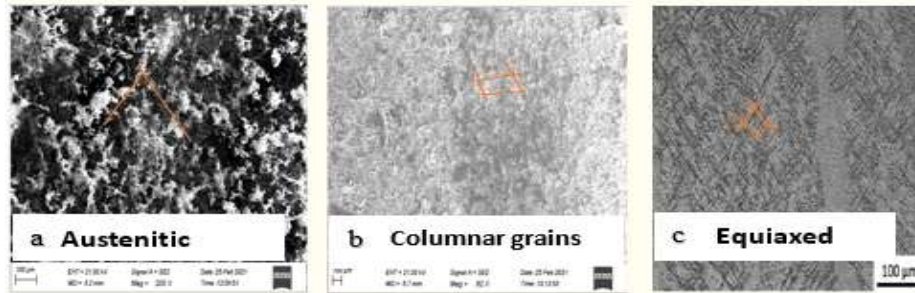


Figure. 8 Optical micrograph of HA-C coating on (a) SS 316L, (b) CoCrMo, (c) Ti6Al4V

Figure 9 shows the XRD spectra of samples with HA-C coatings that were put through a wet (SBF) test. Regarding coating HA is present at every peak. All reinforced HA coatings exhibit a single narrow, tiny CaO peak, confirming the extremely slight presence of amorphous CaO. Tetra calcium phosphate (TTCP) and tricalcium phosphate (-TCP, -TCP) peaks with an angle range of 290 ° to 320 ° are present on all as-sprayed coatings, which is a significant finding. The original powders lack these steps. Because of the amorphous phase's quick solubility in the physiological environment of the human body, the implant suffered a serious failure and was destroyed. The crystalline materials during spray coating are shown to have corroded into the amorphous phase by the sharp HA peaks in the XRD study, which then become broader following coating

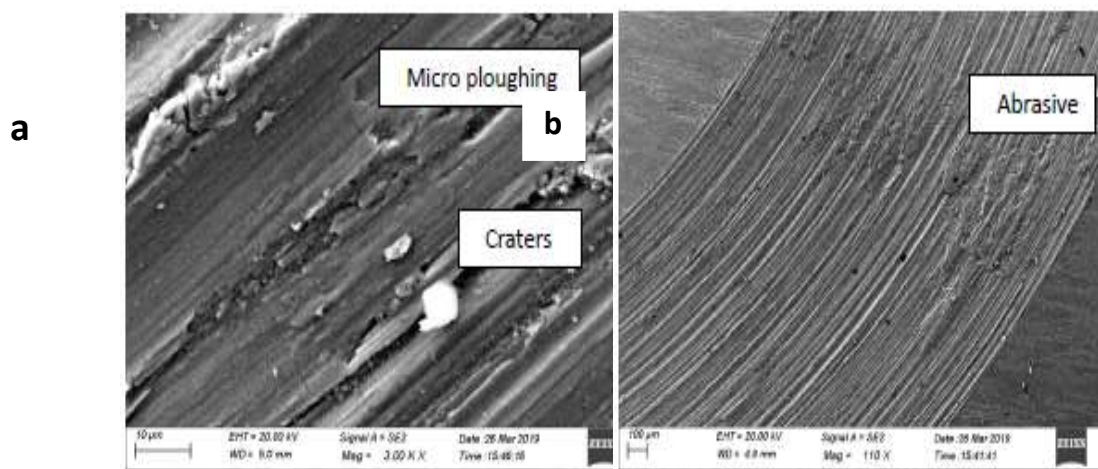


Figure. 9 XRD pattern for plasma sprayed reinforced HA-C coated wet samples (a- 10 wt% & b- 5 wt% wet) HA, a- (a) Austenitic grains (b) Columnar grains (c) Equiaxed

3.2 Sliding wear and Corrosion performance: The findings from the sliding wear experimental are used in this section to elaborate on corrosion behavior and wear mechanism.



3.2.1 Abrasive wear and friction of uncoated and coated with APS specimens against steel: The two key factors influencing a coating's wear resistance are its morphological structure and hardness. Figure 10 (a & b) shows a micrograph image of the wear mechanism on a Ti sample during uniform directional sliding of a specimen coated with HA-C. Uniform and continuous wear is visible in the SEM micrograph taken after the wear test exposure. The abrasive action on both the coated and uncoated surfaces can be seen to leave wear tracks that are visible. Abrasion-induced tiny debris is also visible in the micrograph. As a result of plastic deformation brought on by abrasive wear, SEM images showed the presence of areas with cracks and fractures [33]. Smaller craters and a sizable portion of the surface are shown in the HA-CNT wear track image. The crater is created by chipping and breaking, while the rough surface is produced by abrasive wear.



8417

Figure. 10 Wear scar micrograph of APS- sprayed HA-C coatings against steel ball (a- wear mechanism & b- wear path).

Average weight loss (kg/m^2) for the untreated samples was 0.14, 0.12, and 0.09 kg/m^2 , whereas it was 0.24, 0.22, and 0.18 kg/m^2 for the reinforced HA-C coating. The weight loss of metallic substrates is considerably less than that of all as-sprayed coatings on alloy substrates, as can be seen from the wear findings. The data from Figure 11 can be plotted to show that the wear volume was reduced by up to 75% while the wear resistance of reinforced HA-C coatings with 10wt% and 5wt% reinforcement improved. Increased elastic modulus and fracture toughness are to blame for this improvement.



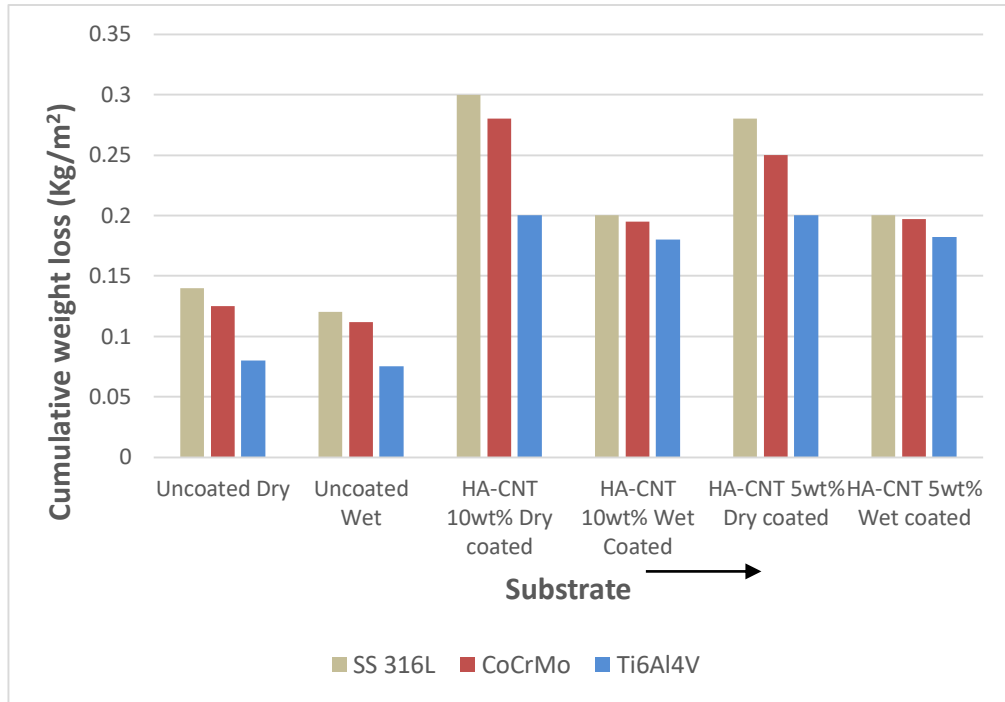


Figure. 11. Variation in wear loss (kg/m^2) of uncoated, 10wt% and 5wt% HA-C coatings alloy in dry and wet (SBF) condition.

Surface hardness, toughness, spraying technique, and contact pressure are thought to be the major influencing variables on the coefficient of friction value. Due to the steel ball's variable contact pressure, Figure 12 shows the cumulative mean CoF ranging from 0.35 to 0.42. For the Ti coated samples under wet (SBF) circumstances, the spray approach has a negative impact on mean CoF, which has decreased up to 0.37. The results of the total mass loss investigation and the 3D analysis of the wear track geometry both supported the conclusion that the presence of PBS in the electrolyte solution tends to accelerate the deterioration of the alloy under the investigated conditions. Since the hardness of the counter body controls tribological failure, it mostly affects the particular wear rate. The Ti6Al4V alloy outperformed all bare and coated specimens in terms of wear resistance. With the addition of reinforcement, wear resistance in the case of HA coatings may be improved. With the

inclusion of reinforced CNT in the HA matrix, the CoF somewhat drops from 0.8 to 0.06. The CoF value decreases as the graphene layer is pulled away from the CNT surface because it provides lubrication.

To remove the single graphite layer from a multiwalled CNT along its axial direction, a tensile stress greater than 11 GPa is necessary [34]. In the current work, the estimated tensile stress in the wear track was 12 GPa, which was discovered to be adequate for stripping the graphene layer from CNT. When the test was run in an SBF-immersed solution, similar outcomes were observed. As the bodily fluid would provide more lubrication on the implant surface, it would also help to reduce wear debris, which would result in improved coating performance inside the human body. Tribo Abrasion, adhesion, and cracking are examples of mechanical wear, which is the most frequent wear process [35].



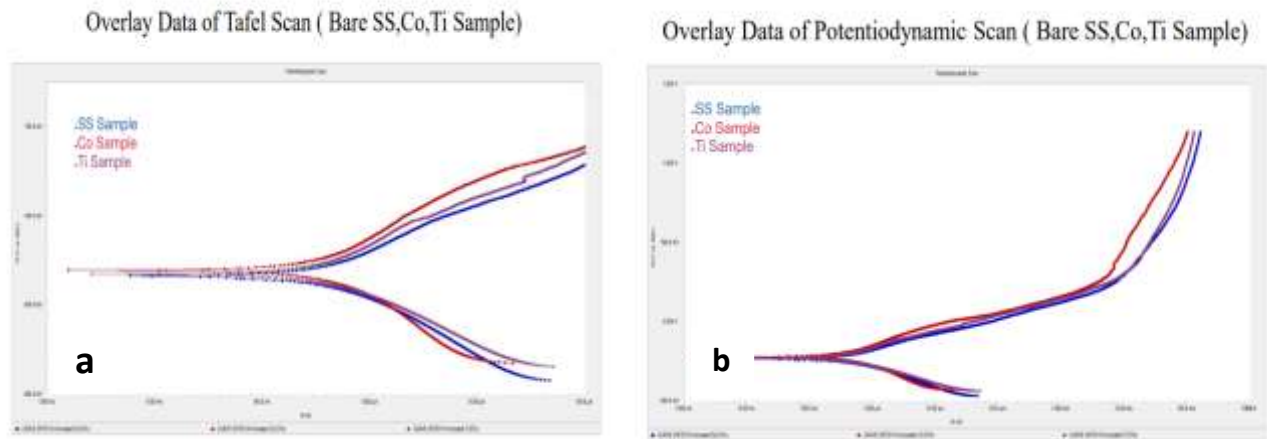
Figure. 12 Average CoF curves for APS coating against steel ball SAE 52100 at contact pressure of 2000 MPa. (a- Sliding Distance Vs CoF & b- Time Vs CoF Curve).

3

.2.2 Corrosion (electrochemical Polarization) Test:

All coated samples' corrosion behavior is assessed using an electrochemical polarization test in a simulated fluid, as suggested by Takadama and Kokubo [36]. Tafel polarization was primarily used to assess the corrosion current density of each and every HA-CNT whereas Potentiodynamic measurements were used to examine the passive behavior of the coatings in simulated bodily fluids coatings. Tafel polarization measurements were performed at a scan rate of 1 mV/s, commencing from -250_{OCP} mV to $+250_{OCP}$ mV. While Potentiodynamic polarization was done starting at -250_{OCP} mV and going all the way up to 1600_{SCE} mV.

Tafel polarization curves of bare SS-316L; Ti6Al4V and CoCrMo alloy substrates are presented in Figure 13. The ranges of passivation potential for bare substrates are -660 mV to -160 mV, -600 mV to -100 mV and -610 mV to 115 mV respectively. Results of polarization test in SBF solution are reported in Table 2. As it is evident that from the Table 2 that corrosion current in case of SS-316L, CoCrMo is more as compared to Ti6Al4V, hence it can be inferred that corrosion resistance of Ti6Al4V is more than that of SS-316L and CoCrMo. Also the passivation range for bare Ti6Al4V is comparatively larger than that of bare SS-316L and CoCrMo.



8419

Figure 13. (a-Overlay Data of Tafel Scan and b-Overlay Data of Potentiodynamic Scan) Tafel polarization curves of bare substrate.

Table 2. Result of Tafel polarization test of Bare SS-316L, Ti6Al4V and CoCrMo in SBF solution.

Specimen	E Corr. (mV)	I Corr. (µA)	β_a (mV)	β_c (mV)
SS-316L (Bare substrate)	-412.218	2.543	390.532	298.390
Ti6Al4V (Bare substrate)	-296.877	0.838	211.516	127.728
CoCrMo (Bare substrate)	-367.209	1.603	297.640	201.428

Likewise Tafel polarization curve of reinforced HA-CNT coatings are shown in Figure 14. The range of passivation potential for as sprayed reinforced HA-
 eISSN1303-5150

CNT coatings is shown in Figure 14 respectively. Results of polarization test are reported in Table 3. It may be observed from the Table 3 that corrosion



current density of almost all coatings is not varying greatly, it varies between 0.637 – 2.54 (μm). In case of as sprayed coatings, corrosion resistance of HA coating has been slightly improved after

incorporating reinforcement. Also reinforced HA-CNT coatings show passive behavior in simulated body fluid which supports the low current density values presented by Tafel polarization method.

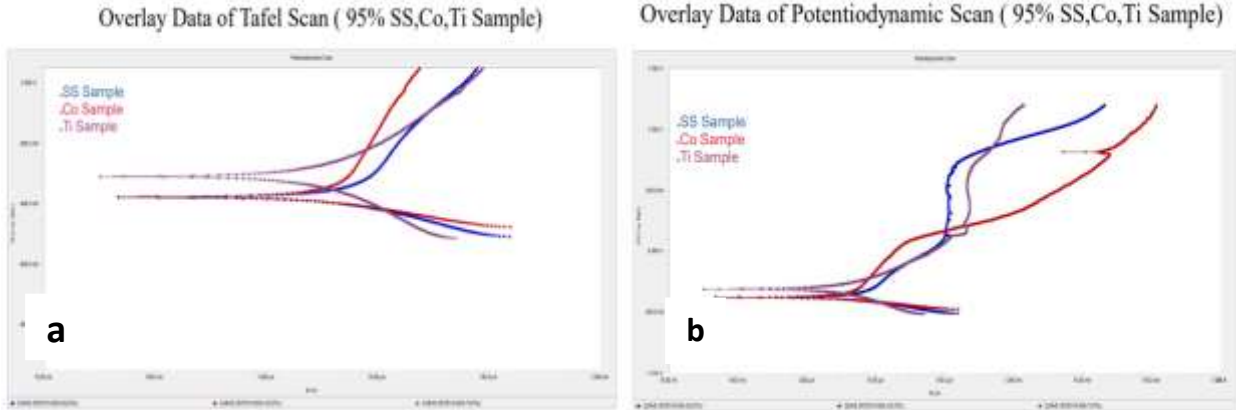


Figure 14. (a-Overlay Data of Tafel Scan and b-Overlay Data of Potentiodynamic Scan) Tafel polarization curves of HA-CNT reinforced substrate.

Table 3. Result of Tafel polarization test of HA-CNT reinforced SS-316L, Ti6Al4V and CoCrMo in SBF solution.

Specimen	E Corr. (mV)	I Corr. (μA)	β_a (mV)	β_c (mV)
SS-316L (Reinforced)	-241.011	2.190	117.600	203.610
Ti6Al4V (Reinforced)	-208.233	0.637	84.833	153.901
CoCrMo (Reinforced)	-221.065	1.217	139.508	142.888

4. **CONCLUSION:** The HA-CNT coating with different wt. % was processed by air plasma spray on alloy samples. The corrosion behavior, characterization and wear properties comparatively were investigated:

- The air plasma spraying technique could be used to successfully create HA-CNT composites. Densification has not been negatively impacted by reinforced CNT. Because of the strong electrical and thermal conductivity of nanotubes, the hydroxyapatite microstructure is more uniform and has enhanced densification.
- The well-retained peeled-off graphene layers allowed for a computed tensile stress in the wear track of about 12 GPa. The morphological structures produced by the 10wt% and 5wt% HA-C coatings are both dense. The cracks were

properly bridged and the fracture energy was entirely absorbed, leading to a better hardening mechanism, because of the high interstitial bonding of HA with the CNT matrix.

- The wear processes of the APS-sprayed HA-C coating on CoCrMo and SS 316 L revealed that a little degree of carbon adhesion and austenitic grain plastic deformation occurred as a result of greater contact stress. The coatings on Ti6Al4V, on the other hand, showed signs of brittle cracking, spalling, and abrasive grooves.
- The addition of 10 weight percent and 5 weight percent CNT reinforcement to plasma spray HA coating resulted in an increase in wear resistance of 75% with a decrease in the amount of wear debris generation. The CoF on the coated surface is reduced by the



lubrication offered by the peeled-off graphene layer from CNT. The size of the wear particles is decreased by CNT presence (HA-CNT: 0.15–3.4 μm).

- Comparisons are made between the corrosion current (I_{corr}) values of the uncoated SS-316L, CoCrMo, and Ti6Al4V alloys and the coatings of HA-CNT sprayed on these substrates. Due to the I_{corr} value of this alloy being the highest among all substrates and HA coatings, bare SS-316L alloy has demonstrated relatively low corrosion resistance. The bare alloys' corrosion resistance in SBF solution can be arranged as follows:

Ti6Al4V > CoCrMo > SS316L

- Of all the HA-CNT coated and uncoated specimens, SS-316L has demonstrated the least amount of corrosion resistance. For biomedical applications, all Coatings have I_{corr} values below 1.6 μA , which can be disregarded. Surgical stainless steel grades have been demonstrated via clinical experience to be vulnerable to localized corrosion in the human body, which results in the release of metal ions into the tissues around the implants. Numerous instances of these devices failing have necessitated the use of biocompatible and corrosion-resistant coatings as well as alloy surface modification.

ACKNOWLEDGEMENT: The authors would like to express their gratitude to Plasma Spray Coats in Bangalore, India, for providing the coating facility. The authors would like to thank VJTI, Mumbai, as well as IIT Bombay, India, for providing testing facilities such as SEM, EDX, XRD, Nano-indentation, and Non-contact profilometer. A special extended thanks to Shree Chitra Tirunal Institute of Medical Science and Technology, Kerala for helping in performing the in-vitro biocompatibility test. This research is not supported by any financial grant from a public or private funding agency.

Disclosure statement: No potential conflict of interest was reported by the author(s).

REFERENCES:

- [1] Mars G. Fontana & Norbert D. Greene (1967), Corrosion and anti-corrosives, Abe Books, McGraw-Hill Series in Materials Science and Engineering, pg 1-391, ISBN 0-07-021463-8.
- [2] Scott P. Patterson, Richard H. Daffner & Robert A. Gallo, (2005), Electrochemical Corrosion of Metal Implants, pg 1219-122, ISBN 0361–803X/05/1844–1219.
- [3] Rana Afif Majed Anaee, (2015), Corrosion Behavior of Some Implant Alloys in Simulated Human Body Environment, PhD Thesis University of Technology, Iraq, Chapter 1, pg 1-112.
- [4] Douglas C. Hansen, (2008), Metal Corrosion in the Human Body: The Ultimate Bio-Corrosion Scenario, The Electrochemical Society Interface, pg 31-34. https://www.electrochem.org/dl/interface/sum/sum08/su08_p31-34.
- [5] Hansen, D.C. (2008). Metal corrosion in the human body: The ultimate bio-corrosion scenario. The Electrochemical Society Interface, 17(2): 31-34. <https://doi.org/10.1149/2.F04082IF>.
- [6] Kamachimudali, U., Sridhar, T.M., Raj, B. (2003). Corrosion of bio implants. Sadhana, 28(3): 601-637. <https://doi.org/10.1007/BF02706450>.
- [7] Arumugam, S., Ju, Y. (2021). Carbon nanotubes reinforced with natural/synthetic polymers to mimic the extracellular matrices of bone—A review. Materials Today Chemistry, 20: 100420. <https://doi.org/10.1016/j.mtchem.2020.100420>.
- [8] Zheng, X.B., Huang, M.H., Ding, C.X. (2000). Bond composite coatings. Biomaterials, 21(8): 841-849. [https://doi.org/10.1016/S0142-9612\(99\)00255-0](https://doi.org/10.1016/S0142-9612(99)00255-0)
- [9] Balani, K., Anderson, R., Laha, T., Andara, M. 8421, Tercero, J., Crumpler, E., Agarwal, A. (2007). hydroxyapatite coatings and their interaction with human osteoblasts in vitro. Biomaterials, 28(4): 618-624. <https://doi.org/10.1016/j.biomaterials.2006.09.013>



- [10] Gopi, D., Shinyjoy, E., Sekar, M., Surendiran, M., Kavitha, L., Kumar, T.S. (2013). Development of carbon nanotubes reinforced hydroxyapatite composite coatings on titanium by electrodeposition method. *Corrosion Science, Biotechnology and Biomaterials*, 1016/j.corsci.2013. 04.021.
- [11] Zalnezhad, E., Musharavati, F., Chen, T., Jaber, F., Uzun, K., Chowdhury, M.E.H., Khandakar, A., Liu, J.X., Bae, S. (2021). Tribo-mechanical properties evaluation of HA/TiO₂/CNT nanocomposite. *Scientific reports*, 11(1): 1-15. <https://doi.org/10.1038/s41598-021-81187-7>.
- [12] Huang, B. (2020). Carbon nanotubes and their polymeric composites: The applications in tissue engineering. *Bio manufacturing Reviews*, 5(1): 1-26. <https://doi.org/10.1007/s40898-020-00009-x>.
- [13] Godwin, G., Jaisingh, S.J., Priyan, M.S., Singh, S.C.E. (2021). Wear and corrosion behaviour of Ti-based coating on biomedical implants. *Surface Engineering*, 37(1): 32-41. <https://doi.org/10.1080/02670844.2020.1730058>.
- [14] Liu, Y., Fischer, T.E., Dent, A. (2003). Comparison of HVOF and plasma-sprayed alumina/titania coatings—microstructure, mechanical properties and abrasion behavior. *Surface and Coatings Technology*, 167(1): 68-76. [https://doi.org/10.1016/S0257-8972\(02\)00890-3](https://doi.org/10.1016/S0257-8972(02)00890-3).
- [15] Gell, M., Jordan, E.H., Sohn, Y.H., Goberman, D., Shaw, L., Xiao, TD. (2001). Development and implementation of plasma sprayed nanostructured ceramic coatings. *Surface and Coatings Technology*, 146: 48-54. [https://doi.org/10.1016/S0257-8972\(01\)01470-0](https://doi.org/10.1016/S0257-8972(01)01470-0).
- [16] Coathup, M.J., Blackburn, J., Goodship, A.E., Cunningham, J.L., Smith, T., Blunn, G.W. (2005). Role of hydroxyapatite coating in resisting wear particle migration and osteolysis around acetabular components. *Biomaterials*, 26(19): 4161-4169. <https://doi.org/10.1016/j.biomaterials.2004.10.020>.
- [17] De Menezes, B.R.C., Rodrigues, K.F., da Silva Fonseca, B.C., Ribas, R.G., do Amaral Montanheiro, T.L., Thim, G.P. (2019). Recent advances in the use of carbon nanotubes of Materials Chemistry B, 7(9): 1343-1360. <https://doi.org/10.1039/C8TB02419G>.
- [18] Wang, Z., Li, Y., Huang, W., Chen, X., He, H. (2016). Micro-abrasion–corrosion behaviour of a biomedical Ti–25Nb–3Mo–3Zr–2Sn alloy in simulated physiological fluid. *Journal of the Mechanical Behavior of Biomedical Materials*, 63: 361-374. <https://doi.org/10.1016/j.jmbbm.2016.07.010>.
- [19] V. Stoilov & D. O. Northwood (2014). Friction Wear and Corrosion: Learning from the nature, *Int. J. Of. Design & Nature and Ecodynamics*, Vol 9, no. 4. 276-284. <https://www.researchgate.net/publication/270591462>.
- [20] Luo, W., Kuai, J. (2018). Friction and wear properties of artificial joints of CoCrMo alloy. In *IOP Conference Series: Materials* 042072. <https://doi.org/10.3390/lubricants8050061>.
- [21] Fellah, M., Labaïz, M., Assala, O., Iost, A., Dekhil, L. (2013). Tribological behaviour of AISI 316L stainless steel for biomedical applications. *Tribology-Materials, Surfaces & Interfaces*, 7(3): 135-149. <https://doi.org/10.1179/1751584X13Y.0000000032>.
- [22] Wu, S., Liu, X., Yeung, K.W.K., Xu, Z.S., Chung, C.Y., Chu, P.K. (2012). Wear properties of porous NiTi orthopedic shape memory alloy. *Journal of materials engineering and performance*, 21(12): 2622-2627. <https://doi.org/10.1007/s11665-012-0392-z>.
- [23] Kokubo, T., Takadama, H. (2006). How useful is SBF in predicting in vivo bone bioactivity?. *Biomaterials*, 27(15): 2907-2915. <https://doi.org/10.1016/j.biomaterials.2006.01.017>.



- [24] Awwaluddin, M., Prajitno, D.H., Adi, W.A., Kartaman, M., Soemardi, T.P. (2020). Mechanical properties and corrosion behavior of novel β -type biomaterial Zr-6Mo-4Ti-xY alloys in simulated body fluid Ringer's lactate solution for implant applications. *AIMS Materials Science*, 7(6): 887-901.
- [25] Luo, W., Kuai, J. (2018). Friction and wear properties of artificial joints of CoCrMo alloy. In *IOP Conference Series: Materials Science and Engineering*, 439(4): 042072. <https://doi.org/10.3390/lubricants8050061>.
- [26] Fellah, M., Labaïz, M., Assala, O., Iost, A., Dekhil, L. (2013). Tribological behavior of AISI 316L stainless steel for biomedical applications. *Tribology-Materials, Surfaces & Interfaces*, 7(3): 135-149. <https://doi.org/10.1179/1751584X13Y.0000000032>
- [27] Wu, S., Liu, X., Yeung, K.W.K., Xu, Z.S., Chung, C.Y., Chu, P.K. (2012). Wear properties of porous NiTi orthopedic shape memory alloy. *Journal of materials engineering and performance*, 21(12): 2622-2627. <https://doi.org/10.1007/s11665-012-0392-z>
- [28] S.Prashantha, S.M.Shashidhara, U.S.Mallikarjuna, & A.G.Shivasiddaramaiah, (2017), Evaluation of Shape Memory Effect and Wear Properties of Cu-Al-Be Shape Memory Alloys, materialstoday: PROCEEDINGS, Volume 4, Issue 9, Pg 10123-10127, <https://doi.org/10.1016/j.matpr.2017.06.333>.
- [29] Kokubo, T., Takadama, H. (2006). How useful is SBF in predicting in vivo bone bioactivity?. *Biomaterials*, 27(15): 2907-2915. <https://doi.org/10.1016/j.biomaterials.2006.01.017>
- [30] Fellah, M., Labaïz, M., Assala, O. Dekhil, L., Zerniz, N., Iost, A. (2014). Tribological behavior of biomaterial for total hip prosthesis. *Matériaux & Techniques*, 102(6-7): 601. <https://doi.org/10.1051/mattech/2014027>
- [31] Muhammad Awwaluddin, Djoko Hadi Prajitno, Wisnu Ari Adi, Maman Kartaman and Tresna P. Soemardi, (2020), Mechanical properties and corrosion behavior of novel β -type biomaterial Zr-6Mo-4Ti-xY alloys in simulated body fluid Ringer's lactate solution for implant applications. " *AIMS Materials Science*, vol. 7, no. 6, pp. 887+.
- [32] Dey, A., Mukhopadhyay, A.K., Gangadharan, S., Sinha, M.K., Basu, D. (2009). Characterization of microplasma sprayed hydroxyapatite coating. *Journal of Thermal Spray Technology*, 18(4): 578-592. <https://doi.org/10.1007/s11666-009-9386-2>.
- [33] Tranquilli, A.L., Lucino, E., Garzetti, G.G., Romanini, C. (1994). Calcium, phosphorus and magnesium intakes correlate with bone mineral content in postmenopausal women. *Gynecological Endocrinology*, 8(1): 55-58. <https://doi.org/10.3109/09513599409028459>.
- [34] Levingstone, T.J. (2008). Optimisation of plasma sprayed hydroxyapatite coatings (Doctoral dissertation, Dublin City University).
- [35] Solanke, S.G., Gaval, V.R. (2020). Tribological studies of different bioimplant materials for orthopaedic application. *ASM Science Journal*, 13. <https://doi.org/10.32802/asmj.2020.526>
- [36] Levingstone, T.J. (2008). Optimisation of plasma sprayed hydroxyapatite coatings (Doctoral dissertation, Dublin City University).

